

# Nearly Perfectly Matched Layer Boundary Conditions for Operator Upscaling of the Acoustic Wave Equation

Chen Lai · Susan E. Minkoff

the date of receipt and acceptance should be inserted later

**Abstract** Acoustic imaging and sensor modeling are processes that require repeated solution of the acoustic wave equation. Solution of the wave equation can be computationally expensive and memory intensive for large simulation domains. One scheme for speeding up solution of the wave equation is the operator-based upscaling method. The algorithm proceeds in two steps. First, the wave equation is solved for fine grid unknowns internal to coarse blocks assuming the coarse blocks do not need to communicate with neighboring blocks in parallel. Second, these fine grid solutions are used to form a new problem which is solved on the coarse grid. Accurate and efficient wave propagation schemes also must avoid artificial reflections off of the computational domain edges. One popular method for preventing artificial reflections is the Nearly Perfectly Matched Layer (NPML) method. In this paper we discuss applying NPML to operator upscaling for the wave equation. We show that although we only apply NPML to the first step of this two step algorithm (directly affecting the fine grid unknowns only), we still see a significant reduction of reflections back into the domain. We describe three numerical experiments (one homogeneous medium experiment and two heterogeneous media examples) in which we validate that the solution of the wave equation exponentially decays in the NPML re-

---

This research was performed with funding from the National Science Foundation (grant DMS-0714159).

C. Lai  
Department of Mathematics and Statistics, The University of Maryland, Baltimore County, 1000 Hilltop Circle, Baltimore, MD 21250 E-mail: lai1@umbc.edu

S.E. Minkoff  
Department of Mathematical Sciences, The University of Texas at Dallas, 800 West Campbell Road, Richardson, TX 75080-3021 E-mail: sminkoff@utdallas.edu

gions. Numerical experiments of acoustic wave propagation in two dimensions with a reasonable absorbing layer thickness resulted in a maximum pressure reflection of 3–8%. While the coarse grid acceleration is not explicitly damped in our algorithm, the tight coupling between the two steps of the algorithm results in only 0.1–1% of acceleration reflecting back into the computational domain.

**Keywords** nearly perfectly matched layers · absorbing boundary conditions · acoustic wave propagation · upscaling

**Mathematics Subject Classification (2000)** MSC 86–08 · MSC 35L05 · MSC 65M60 · MSC 65M06

## 1 Introduction

In seismic inversion the objective is to determine the mechanical parameters that describe the propagation of waves through the earth by minimizing the misfit between measured seismograms and data predicted by a mathematical model of the earth. At the heart of the inverse problem is a forward model for wave propagation which is solved repeatedly each time an update is made to the earth parameters. Because this iterative process can be costly computationally, it is important to use numerical schemes that define an accurate solution and preclude artificial reflections from the computational domain boundaries especially when realistic physical experiments include seismic sources and receivers placed near the earth's surface and out laterally to the domain edges. Extending the computational domain to avoid reflections off the boundaries is generally prohibitive for realistic wave propagation imaging problems. Earth science modeling is made even

more complex due to the fact that parameters range from the pore scale (millimeters) to the field scale (kilometers). One must make choices about the most important scales on which to focus attention. To address the multiple scale problem, Vodovina, Minkoff, and Korostyshevskaya applied operator-based upscaling to the acoustic wave equation to capture the effect of the fine scales on a coarse-scale solution [33, 31, 26]. This operator-based upscaling method does not produce new effective or equivalent coefficients on the coarse grid, but rather provides an effective solution directly. This method has the advantage that no *a priori* assumptions are made about the medium being periodic or having scale separation.

While upscaling schemes for reservoir simulation have been studied extensively for some time now (see for a small sample, [10, 5, 25, 2, 1]), multiscale techniques for solving the wave equation have only gained attention over the last decade or so. For flow simulation, permeability (an uncertain parameter) can vary over four orders of magnitude locally. While wave parameters (velocity and density) do not fluctuate as extensively, pinpointing the location of interfaces (jumps in material parameters) is of even more importance for exploration seismology than for reservoir simulation. Over the last 10–15 years, attention has focused on methods that attempt to capture sub-wavelength heterogeneities on a coarse scale for wave propagation and imaging (see for example the papers by Chung, Efendiev and Gibson, Engquist, etc. [12, 11, 6, 14, 34]). Very little of the literature is focused on the development of effective absorbing boundary conditions for these multiscale techniques.

Operator-based upscaling was originally developed for fluid flow (see [2]). Minkoff and collaborators have since applied and studied the implementation of the upscaling method for both the acoustic and elastic wave equations (see [33, 26, 31, 32]) as well as for imaging [28]. The method uses a two-scale decomposition of the solution, and it has been shown to accurately capture fine-scale heterogeneities in the upscaled solution and to exhibit nearly ideal speedup with no communication between processors [33]. The fine grid solve is the expensive part of the algorithm and is, therefore, where the savings occurs. The coarse problem is generally quite small and can often be solved in serial.

Absorbing boundaries can be categorized into two broad categories: rigorous “non-local” boundaries [16] and approximate “local” boundaries [7]. The rigorous non-local boundaries are highly accurate and often formulated for time-harmonic problems [15]. Approximate local absorbing boundaries can be formulated for transient problems [17] at low computational cost. In practice,

these boundary conditions do not result in perfect absorption. Ideally, absorbing boundaries should absorb waves independent of frequency and incidence angle [27, 18]. Berenger introduced the concept of “Perfectly Matched Layer” conditions (PML) for Maxwell’s equations [3]. “Perfectly matching” implies that the interface between the computational domain and the absorbing layer does not exhibit any reflection. PML attempts to eliminate reflected waves from all non-tangential angles-of-incidence and frequency. PML boundary conditions have been applied extensively to computational electromagnetism, the scalar Helmholtz equation, advective acoustics, poroelastic media, shallow water waves, elasticity, and others (see for example [24, 4, 20, 3, 16, 7]). Cummer reformulated PML for Maxwell’s equations in such a way that the governing equations in any linear media did not change [9]. This formulation is called Nearly Perfectly Matched Layers (or NPML). The method was applied to first-order equations arising in seismic modeling by Hu and Cummer [19]. *In this work we investigate NPML for operator upscaling applied to the acoustic wave equation.* In this paper we start by reviewing operator upscaling. We then show how to apply NPML to our formulation of the wave equation as a second-order system in space and then to the discrete form that results from operator upscaling. We conclude with numerical experiments showing the effectiveness of NPML for operator upscaling applied to acoustics.

## 2 Operator-Based Upscaling of the 2-D Acoustic Wave Equation: Background

The study of upscaling methods is driven by the need to develop numerical schemes which capture fine-scale solution detail in a coarse scale solution to save on storage and computation time. Upscaling traditionally has involved redefining the physical system parameters on a coarser grid [5, 10, 25]. We will now review operator (or subgrid) upscaling which does not redefine input parameters in the model but instead determines an upscaled solution directly. This review summarizes Vodovina, Korostyshevskaya and Minkoff [33, 26]. We start by assuming the computational grid contains unknowns which live on both a coarse and a fine (or subgrid) scale. The problem is solved first for the fine grid unknowns within each coarse block and then this subgrid solution is used to define an upscaled solution operator on the coarse grid.

Let  $\Omega$  be a two-dimensional domain with boundary  $\Gamma$ . We consider the acoustic wave equation in  $\Omega$  written as the (non-standard) first-order system in space for

acceleration  $\mathbf{v}$  and pressure  $p$ :

$$\begin{aligned} \mathbf{v} &= -\frac{1}{\rho} \nabla p && \text{in } \Omega, \\ \frac{1}{\rho c^2} \frac{\partial^2 p}{\partial t^2} &= -\nabla \cdot \mathbf{v} + f \text{ in } \Omega, \end{aligned} \quad (1)$$

Here  $c$  is the sound velocity,  $\rho$  is the density, and  $f$  is the source of acoustic energy.

The subgrid upscaling technique is based on a mixed finite element variational formulation of these equations. Let  $H_0(\text{div}; \Omega)$  be the set of vector functions,  $\mathbf{v}$ , such that:

$$\{\mathbf{v} \in (L^2(\Omega))^2 : \nabla \cdot \mathbf{v} \in L^2(\Omega), \text{ and } \mathbf{v} \cdot \nu = 0 \text{ on } \Gamma\},$$

where  $\nu$  is the unit outward normal to the boundary  $\Gamma$ . Rewriting System (1) in weak form we would like to find  $\mathbf{v} \in H_0(\text{div}; \Omega)$  and  $p \in L^2(\Omega)$  such that

$$\begin{aligned} \langle \rho \mathbf{v}, \mathbf{u} \rangle &= \langle p, \nabla \cdot \mathbf{u} \rangle, \\ \left\langle \frac{1}{\rho c^2} \frac{\partial^2 p}{\partial t^2}, w \right\rangle &= -\langle \nabla \cdot \mathbf{v}, w \rangle + \langle f, w \rangle, \end{aligned} \quad (2)$$

for all  $\mathbf{u} \in H_0(\text{div}; \Omega)$  and  $w \in L^2(\Omega)$ . The two-dimensional domain  $\Omega$  is decomposed into a coarse mesh, and each coarse element  $E^c$  is further decomposed into a subgrid mesh. While alternate formulations are certainly possible (see for example, our upscaling of the elastic wave equation where all unknowns are upscaled [32] and the earlier work by Arbogast et al. [2] in which both pressure and velocity are upscaled for flow), in this work we only upscale acceleration. The implementation of NPML that we describe here is a practical necessity that applies to the algorithm we have analyzed and implemented in related papers such as [33, 26, 31]. The space of acceleration unknowns can be decomposed uniquely into the sum  $\mathbf{v} = \mathbf{v}^c + \delta\mathbf{v}$  where the coarse acceleration is denoted by  $\mathbf{v}^c$  and the fine-grid acceleration internal to each coarse-grid cell is  $\delta\mathbf{v}$ . Both of these spaces consist of vector functions living on the edges of the grid blocks (see Figure 1).

In the subgrid upscaling method we describe here, both the coarse and fine components of the horizontal acceleration are approximated by the space of piecewise continuous linear functions in  $x$  and piecewise constants in  $y$  (for vertical acceleration we use linear functions in  $y$  and constants in  $x$ ). The coarse and subgrid basis functions  $(u_x^c)_i, (\delta u_x)_i$  for acceleration have nodes at the midpoints of vertical edges of the coarse and fine cells respectively (Figure 1). The pressure  $p$  is approximated by piecewise constants defined on the fine grid with nodes at the centers of the fine cells.

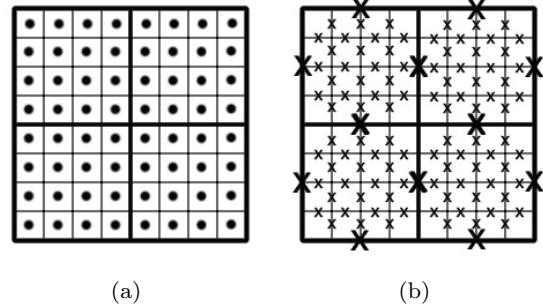


Fig. 1: A sample domain  $\Omega$  consisting of 4 coarse cells. Each coarse cell contains 16 fine-grid blocks. (a) The dots represent nodes for the pressure space  $\delta W$ . (b) The large crosses represent nodes for the coarse acceleration space  $V^c$ , and the small crosses represent nodes for the subgrid acceleration space  $\delta V$ .

In order to decouple the subgrid problems from coarse block to coarse block, homogeneous Neumann boundary conditions are imposed on each coarse block:

$$\delta \mathbf{u} \cdot \nu = 0 \quad \text{on } \partial E^c. \quad (3)$$

*This is the primary simplifying assumption in the definition of the operator-based upscaling method.* This condition enables an efficient parallel implementation of the method by decoupling the subgrid problems so that no communication between processors is required. The method consists of two steps: (1) finding the solution to the subgrid problems assuming Condition (3) on coarse block edges, and (2) determining the coarse acceleration.

**Step 1:** By choosing test functions which live on the fine grid, we can solve the subgrid problems in terms of the coarse acceleration  $\mathbf{v}^c$ :

$$\langle \rho(\mathbf{v}^c + \delta\mathbf{v}), \delta\mathbf{u} \rangle_{E^c} - \langle p, \nabla \cdot \delta\mathbf{u} \rangle_{E^c} = 0, \quad (4)$$

$$\left\langle \frac{1}{\rho c^2} \frac{\partial^2 p}{\partial t^2}, w \right\rangle_{E^c} + \langle \nabla \cdot (\mathbf{v}^c + \delta\mathbf{v}), w \rangle_{E^c} = 0, \quad (5)$$

for all  $\delta\mathbf{u} \in \delta\mathbf{V}(E^c)$  and  $w \in W(E^c)$ . For simplicity we have dropped the source function  $f$ . Pressure is completely determined by Step 1 of the algorithm. Although the algorithm was developed based on the mixed finite element method, the equivalence between cell-centered finite differences and lowest-order mixed finite elements allows us to solve the expensive subgrid problem via finite differences [29, 33]. In fact Equations (4) and (5) can be discretized using second-order in space and time, staggered finite-differences to give:

$$\begin{aligned} \frac{1}{k_{i+\frac{1}{2},j+\frac{1}{2}}} \frac{p_{i+\frac{1}{2},j+\frac{1}{2}}^{n+1} - 2p_{i+\frac{1}{2},j+\frac{1}{2}}^n + p_{i+\frac{1}{2},j+\frac{1}{2}}^{n-1}}{(\Delta t)^2} \\ = (D_x + D_y)(\delta\mathbf{v} + \mathbf{v}^c)|_{i+\frac{1}{2},j+\frac{1}{2}}^n, \end{aligned} \quad (6)$$

$$\delta v_x|_{i,j+\frac{1}{2}}^{n+1} = -v_x^c|_{i,j+\frac{1}{2}}^{n+1} - D_x p|_{i,j+\frac{1}{2}}^{n+1}, \quad (7)$$

$$\delta v_y|_{i+\frac{1}{2},j}^{n+1} = -v_y^c|_{i+\frac{1}{2},j}^{n+1} - D_y p|_{i+\frac{1}{2},j}^{n+1}, \quad (8)$$

$$\delta v_x|_{0,j+\frac{1}{2}}^{n+1} = \delta v_x|_{N_x,j+\frac{1}{2}}^{n+1} = 0, \quad (9)$$

$$\delta v_y|_{i+\frac{1}{2},0}^{n+1} = \delta v_y|_{i+\frac{1}{2},N_y}^{n+1} = 0, \quad (10)$$

where  $n$  corresponds to the time level,  $D_x$  and  $D_y$  denote first-order, centered finite difference operators,  $N_x$  and  $N_y$  correspond to the number of fine cells inside each coarse cell in the  $x$  and  $y$  directions, respectively,  $k_{i,j}$  is the bulk modulus, and  $\Delta t$  is the time step.

**Step 2:** Determine coarse acceleration  $\mathbf{v}^c$  by solving

$$\langle \rho(\mathbf{v}^c + \delta\mathbf{v}(\mathbf{v}^c)), \mathbf{u}^c \rangle = \langle p, \nabla \cdot \mathbf{u}^c \rangle, \quad (11)$$

for all  $\mathbf{u}^c \in \mathbf{V}^c$ . Korostyshevskaya and Minkoff [26] proved that the upscaling technique results in the linear system for the coarse acceleration and pressure of the form:

$$U\mathbf{v}_x^c = D\mathbf{p}, \quad (12)$$

where  $U$  is a diagonal matrix of size  $(K-1) \times (K-1)$  where  $K$  is the number of coarse cells in the domain, and  $D$  is a block upper bidiagonal matrix of size  $(K-1) \times n_x n_y K$ . Here  $n_x n_y K$  is the total number of fine cells in the domain. The entries of the matrix  $U$  are given by the sum of density values,  $\rho_l$ , on the corresponding boundaries of the coarse cells:

$$U_{i,i} = (h_x h_y) \sum_l \rho_l^i. \quad (13)$$

The non-zero entries of the matrix  $D$  correspond to the pressure nodes located along the boundaries of the coarse cells (see Figure 2). The matrix Equation (12) for  $\mathbf{v}_x^c$  and  $\mathbf{p}$  gives us insight into the equations solved by the upscaling algorithm and greatly simplifies the implementation of the method. Thus substituting in the expressions for  $U$  and  $D$  into Equation (12) gives the difference equation for coarse acceleration in the NPML region as:

$$(h_x h_y) \sum_{l=1}^{n_y} \rho_l^i (\mathbf{v}_x^c)_i = -(h_x h_y) \left[ \sum_{l=1}^{n_y} \frac{\mathbf{p}_{N_i+n_x(l-1)+1}}{h_x} - \sum_{l=1}^{n_y} \frac{\mathbf{p}_{N(i-1)+n_x l}}{h_x} \right]. \quad (14)$$

Here  $h_x$  and  $h_y$  denote the spatial grid spacing in the  $x$  and  $y$  directions, respectively. Notice that the coarse

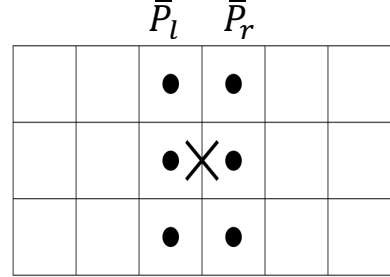


Fig. 2: Two adjacent  $3 \times 3$  coarse grid cells with the coarse acceleration unknown represented by the cross. Pressure nodes are shown as dots.

acceleration is only dependent on pressure and the average of the density values on the boundary of the coarse cell. In our NPML implementation for upscaling we will, therefore, choose to only damp pressure and sub-grid acceleration in Step 1 of the algorithm. We do not explicitly apply NPML to Step 2 of the upscaling algorithm.

### 3 Nearly Perfectly Matched Layers for the 2-D Acoustic Wave Equation

#### 3.1 NPML for the Alternative Formulation of the Acoustic Wave Equation

Hu, Abubakar, and Habashy [20] applied NPML to acoustic wave propagation with the governing equations given by Fokkema and van den Berg [13], and showed the equivalence of the PML and NPML formulations in 3-D Cartesian coordinates. Johnson notes [22] that all wave equations, from scalar waves to Maxwell's equations can be written in the abstract form

$$\partial \mathbf{w} / \partial t = \hat{D} \mathbf{w} \quad (15)$$

for some wave function  $\mathbf{w}(\mathbf{x}, t)$  and some anti-Hermitian operator  $\hat{D}$ . The same PML ideas apply equally well in all of these cases. In this section we show how to apply NPML to our alternative formulation of the 2-D acoustic wave equation given as a first-order system in space, not time (System (1)), as this is the formulation used in the upscaling algorithm. This is a non-standard form of the wave equation and hence worth examining even in the continuous case in the context of how one would apply NPML. The frequency domain version of System (1) can be found by taking the Fourier transform in time and using the Fourier derivative theorem ( $(\frac{\partial^n}{\partial t^n} f(t)) \Leftrightarrow (i\omega)^n F(s)$ ) [23] to get:

$$\hat{v}_x = -\frac{1}{\rho} \frac{\partial \hat{p}}{\partial x}, \quad (16)$$

$$\hat{v}_y = -\frac{1}{\rho} \frac{\partial \hat{p}}{\partial y}, \quad (17)$$

$$\frac{1}{pc^2} (-i\omega)^2 \hat{p} = -\left( \frac{\partial \hat{v}_x}{\partial x} + \frac{\partial \hat{v}_y}{\partial y} \right), \quad (18)$$

where  $\hat{v}_x$ ,  $\hat{v}_y$ , and  $\hat{p}$  are the Fourier transform with respect to time of  $v_x$ ,  $v_y$ , and  $p$ , respectively. The mathematically equivalent NPML formulation of Equations (16–18) is:

$$\hat{v}_\alpha = -\frac{1}{\rho} \frac{\partial}{\partial \alpha} \left( \frac{\hat{p}}{\gamma_\alpha} \right), \quad (19)$$

$$\frac{1}{pc^2} (-i\omega)^2 \hat{p} = -\frac{\partial}{\partial x} \left( \frac{\hat{v}_x}{\gamma_x} \right) - \frac{\partial}{\partial y} \left( \frac{\hat{v}_y}{\gamma_y} \right), \quad (20)$$

where  $\alpha$  denotes a spatial component,  $\alpha \in \{x, y\}$ , and  $\gamma_\alpha$  is defined as the complex coordinate stretch factor, i.e.,  $\gamma_\alpha = 1 - i\eta_\alpha/\omega$  as in [20].

While the PML decay factor,  $\eta_\alpha$ , can be defined in several ways, we use the expression given in Hu, Abubakar, and Habashy [20], namely:

$$\eta_\alpha(\alpha) = \begin{cases} \eta [(L - \alpha)/L]^3 & \text{for } \alpha \leq L, \\ 0 & \text{for } L < \alpha \leq L + \alpha_m, \\ \eta [(\alpha - L - \alpha_m)/L]^3 & \text{for } L + \alpha_m \leq \alpha, \end{cases}$$

where  $L$  is the thickness of the NPML layer,  $\eta$  is the maximum NPML decay factor, and  $\alpha_m$  is the size of the physical medium (computational) domain.

Since we wish to solve the equations in the time domain, we use the Fourier inversion formula to transform Equations (19) and (20) back:

$$v_\alpha = -\frac{1}{\rho} \frac{\partial}{\partial \alpha} \left( \frac{p}{\gamma_\alpha} \right), \quad (21)$$

$$\frac{1}{pc^2} \frac{\partial^2 p}{\partial t^2} = -\left( \frac{\partial}{\partial x} \left( \frac{v_x}{\gamma_x} \right) + \frac{\partial}{\partial y} \left( \frac{v_y}{\gamma_y} \right) \right). \quad (22)$$

To simplify the NPML formulation above, we define auxiliary variables by:

$$\bar{p}^\alpha = \frac{p}{\gamma_\alpha}; \quad \bar{v}_\alpha^\alpha = \frac{v_\alpha}{\gamma_\alpha}. \quad (23)$$

Note that the subscript denotes the spatial components. The superscript denotes the spatial components in the complex coordinate stretch factor,  $\gamma_\alpha$ . For instance,  $\bar{v}_y^x$  is the auxiliary acceleration variable in the  $y$ -direction with the complex coordinate stretch factor in the  $x$ -direction. Specifically,  $\bar{v}_y^x = \frac{v_y}{\gamma_x} = v_y/(1 - i\eta_x/\omega)$ .

These auxiliary variables can be substituted into Equations (21) and (22) to obtain the simplified NPML formulation:

$$v_\alpha = -\frac{1}{\rho} \frac{\partial \bar{p}^\alpha}{\partial \alpha}, \quad (24)$$

$$\frac{1}{pc^2} \frac{\partial^2 p}{\partial t^2} = -\frac{\partial}{\partial x} \bar{v}_x^x - \frac{\partial}{\partial y} \bar{v}_y^y. \quad (25)$$

Hu [20] connected the state variables  $\xi$  to the auxiliary state variable  $\bar{\xi}^\alpha$  by augmenting the system with auxiliary differential equations of the form

$$\bar{\xi}^\alpha = \frac{\xi}{1 - i\eta_\alpha/\omega}, \quad (26)$$

where  $\xi \in \{p, v_x, v_y\}$ .

Equation (23) for acceleration can be formulated as follows:

$$v_\alpha = \gamma_\alpha \bar{v}_\alpha^\alpha = \bar{v}_\alpha^\alpha - (i\eta_\alpha/\omega) \bar{v}_\alpha^\alpha. \quad (27)$$

By introducing an auxiliary field variable  $\Phi$  [22] satisfying:

$$-i\omega \Phi = \eta_\alpha \bar{v}_\alpha^\alpha, \quad (28)$$

Equation (27) can be rewritten as:

$$\bar{v}_\alpha^\alpha + \Phi_\alpha = v_\alpha, \quad (29)$$

Moving back to the time domain we, therefore, get

$$\frac{\partial \bar{v}_\alpha^\alpha}{\partial t} + \eta \bar{v}_\alpha^\alpha = \frac{\partial v_\alpha}{\partial t}. \quad (30)$$

Similarly the closure relationship between the original and contracted pressure field is the following:

$$\frac{\partial \bar{p}^\alpha}{\partial t} + \eta_\alpha \bar{p}^\alpha = \frac{\partial p}{\partial t}, \quad (31)$$

where  $\alpha \in \{x, y\}$ .

Equations (24) and (25) along with the auxiliary differential Equations (30) and (31) can be discretized via finite differences as follows:

$$v_{i+1/2,j}^n = -\frac{1}{\rho_{i+1/2,j} h_x} (\bar{p}_{i+1,j}^n - \bar{p}_{i,j}^n), \quad (32)$$

$$v_{i,j+1/2}^n = -\frac{1}{\rho_{i,j+1/2} h_y} (\bar{p}_{i,j+1}^n - \bar{p}_{i,j}^n), \quad (33)$$

$$\begin{aligned} p_{i,j}^{n+1} &= 2p_{i,j}^n - p_{i,j}^{n-1} - \frac{k_{i,j}(\Delta t)^2}{h_x} (\bar{v}_{i+1/2,j}^n - \bar{v}_{i-1/2,j}^n) \\ &\quad - \frac{k_{i,j}(\Delta t)^2}{h_y} (\bar{v}_{i,j+1/2}^n - \bar{v}_{i,j-1/2}^n), \end{aligned} \quad (34)$$

$$\bar{\xi}_{\alpha_{i,j}}^{n+1} = (\xi_{\alpha_{i,j}}^{n+1} - \xi_{\alpha_{i,j}}^n) + \bar{\xi}_{\alpha_{i,j}}^n - \eta_\alpha \Delta t \bar{\xi}_{\alpha_{i,j}}^n, \quad (35)$$

where  $\xi \in \{p, v_x, v_y\}$ . We note that Equations (32–34) have the same form as a finite difference discretization of the original Equations (1). Equation (35) gives three auxiliary ODEs which augment the system for the new NPML implementation.

### 3.2 Implementation of NPML with Operator-Based Upscaling

The NPML formulation is used to attenuate outgoing acoustic waves. Within the computational domain, the NPML formulation does not change the governing equations, hence it is ideal for reusing software which implements complex discretizations such as upscaling.

When we apply these same ideas to determine the NPML formulation of the system of discretized equations that correspond to Step 1 of the upscaling algorithm (6)–(10) we obtain the system:

$$\begin{aligned} \frac{1}{k_{i+\frac{1}{2},j+\frac{1}{2}}} \frac{p_{i+\frac{1}{2},j+\frac{1}{2}}^{n+1} - 2p_{i+\frac{1}{2},j+\frac{1}{2}}^n + p_{i+\frac{1}{2},j+\frac{1}{2}}^{n-1}}{(\Delta t)^2} \\ = (D_x + D_y)(\bar{\mathbf{v}} + \mathbf{v}^c)|_{i+\frac{1}{2},j+\frac{1}{2}}^n, \end{aligned} \quad (36)$$

$$\delta v_x|_{i,j+\frac{1}{2}}^{n+1} = -v_x^c|_{i,j+\frac{1}{2}}^{n+1} - D_x \bar{p}|_{i,j+\frac{1}{2}}^{n+1}, \quad (37)$$

$$\delta v_y|_{i+\frac{1}{2},j}^{n+1} = -v_y^c|_{i+\frac{1}{2},j}^{n+1} - D_y \bar{p}|_{i+\frac{1}{2},j}^{n+1}, \quad (38)$$

$$\delta v_x|_{0,j+\frac{1}{2}}^{n+1} = \delta v_x|_{N_x,j+\frac{1}{2}}^{n+1} = 0, \quad (39)$$

$$\delta v_y|_{i+\frac{1}{2},0}^{n+1} = \delta v_y|_{i+\frac{1}{2},N_y}^{n+1} = 0, \quad (40)$$

$$\bar{p}_{\alpha_{i,j}}^{n+1} = (p_{\alpha_{i,j}}^{n+1} - p_{\alpha_{i,j}}^n) + \bar{p}_{\alpha_{i,j}}^n - \eta_\alpha \Delta t \bar{p}_{\alpha_{i,j}}^n, \quad (41)$$

all 7	$p \ v_x^c \ v_y^c \ \delta v_x \ \delta v_y \ \bar{p} \ \bar{\delta v}_y$	all 7
$v$ $v_x^c \ v_y^c$ $\delta v_x \ \delta v_y$ $\bar{p} \ \bar{\delta v}_x$	Computational Domain	$p$ $v_x^c \ v_y^c$ $\delta v_x \ \delta v_y$ $\bar{p} \ \bar{\delta v}_x$
all 7	$p \ v_x^c \ v_y^c \ \delta v_x \ \delta v_y \ \bar{p} \ \bar{\delta v}_y$	all 7

Fig. 3: 2D acoustic wave equation: The entire domain is discretized into 9 subdomains. Only the state variables are active in the computational domain (shown in white). The state and auxiliary variables are active in the NPML regions (in gray).

$$\bar{\delta v}_{x_{i,j}}^{n+1} = (\delta v_{x_{i,j}}^{n+1} - \delta v_{x_{i,j}}^n) + \bar{\delta v}_{x_{i,j}}^n - \eta_x \Delta t \bar{\delta v}_{x_{i,j}}^n, \quad (42)$$

$$\bar{\delta v}_{y_{i,j}}^{n+1} = (\delta v_{y_{i,j}}^{n+1} - \delta v_{y_{i,j}}^n) + \bar{\delta v}_{y_{i,j}}^n - \eta_y \Delta t \bar{\delta v}_{y_{i,j}}^n, \quad (43)$$

where  $\{\bar{p}, \bar{\delta v}_x, \bar{\delta v}_y\}$  are the auxiliary variables. In this system of differential equations, we introduced three auxiliary variables and three auxiliary differential equations.

To determine the effect of the auxiliary variables, we note from Figure 3 that the auxiliary variables are active from the three additional auxiliary differential equations in the NPML regions. The final NPML formulation above does not change the form of the original governing equations in the computational domain.

## 4 Numerical Experiments

In this section we illustrate via numerical experiments the effectiveness of our NPML implementation in the context of operator upscaling. While it is rarely the case that all reflections are damped completely with PML or NPML even with standard discretizations of the wave equation, it does appear this implementation effectively damps the majority of the reflected wave for both pressure and acceleration. The experiments we present in

this section include NPML applied to a standard staggered grid finite difference discretization of our first-order acoustic system (Equations (1)) as well as the operator upscaling algorithm with and without NPML. Our focus in this work is to understand NPML in the context of upscaling for the wave equation. However, we show the staggered grid finite difference solution simply for comparison since it is a more standard discretization of the wave equation.

Two important considerations for numerical solution of the wave equation are stability and dispersion. Vdovina, Minkoff, and Korostyshevskaya [33] showed that if

$$c_o^2 \Delta t^2 \left( \frac{1}{\Delta x^2} + \frac{1}{\Delta y^2} \right) < 1, \quad (44)$$

then the discrete energy is positive. So temporal iterates are bounded by the initial data and the discrete upscaling scheme is stable. This stability condition corresponds to the standard CFL condition for the acoustic wave equation. Here we have denoted the length of a single fine cell in the  $x$  and  $y$  directions by  $\Delta x$  and  $\Delta y$ , respectively. The fine-grid time step is denoted by  $\Delta t$ , and  $c_0$  is a lower bound on the sound velocity. To minimize the effect of numerical dispersion, at least 10 grid points per wavelength is required for the standard second-order in time and space numerical scheme [8]. Vdovina et al. [33] confirmed numerically that this number of grid points per wavelength appears satisfactory for the upscaling algorithm. In our experiments a single coarse block contains 10 fine grid blocks in  $x$  and 10 in  $y$ . Hence, 100 fine-grid and 10 coarse-grid nodes per wavelength are used in these experiments.

In all of our upscaling experiments, the computational domain is 1.7 km by 1.7 km (1700 x 1700 fine grid points, 170 x 170 coarse grid points). The spatial grid spacing is  $\Delta x = h_x = 1$  m and  $\Delta y = h_y = 1$  m, and the time step is chosen to satisfy the CFL condition. In all experiments, the 2-D Gaussian source function

$$f(x, y) = \frac{1}{\sqrt{(2\pi\sigma^2)}} \exp \left( -\frac{(x - x_0)^2 + (y - y_0)^2}{2\sigma^2} \right) \quad (45)$$

is used, where  $\sigma$  controls the wavelength. Here the source is located at  $(x_0, y_0) = (850m, 850m)$  (the center of the computational domain), and  $\sigma = 100m$ . We note that the source is implemented as an initial condition in the code. In order to reduce reflections while minimizing the size of the absorbing layer, the NPML region is chosen to be 150 fine grid points on each of the four

edges of the computational domain. Thus the total domain (computational plus absorbing layer) is 2 km x 2 km (2000 x 2000 fine grid points, 200 x 200 coarse grid points).

#### 4.1 Homogeneous Medium Experiments

For the homogeneous medium experiments, the sound velocity is 2500 m/s, and the time step is  $\Delta t = 3.42 \times 10^{-4}$  s which satisfies the CFL condition. The incident pressure wave reaches the edges of the computational domain at time  $t = 0.342$  s (the 1000th time step). The maximum NPML decay factor,  $\eta$ , was chosen to have value 250. Later we present experiments in which we vary both the layer thickness and the absorption coefficient and indicate why we chose these values as optimal.

We begin by showing results obtained using NPML with the standard staggered grid finite difference (SGFD) scheme but without upscaling. The scheme is a second-order centered finite difference approximation in both space and time for System (1). The staggered grid is shown in Figure 4, and the discretization of the equations is given by

$$v_{i+1/2,j}^n = -\frac{1}{\rho_{i+1/2,j} h_x} (p_{i+1,j}^n - p_{i,j}^n), \quad (46)$$

$$v_{i,j+1/2}^n = -\frac{1}{\rho_{i,j+1/2} h_y} (p_{i,j+1}^n - p_{i,j}^n), \quad (47)$$

$$\begin{aligned} p_{i,j}^{n+1} = 2p_{i,j}^n - p_{i,j}^{n-1} - \frac{k_{i,j}(\Delta t)^2}{h_x} (v_{i+1/2,j}^n - v_{i-1/2,j}^n) \\ - \frac{k_{i,j}(\Delta t)^2}{h_y} (v_{i,j+1/2}^n - v_{i,j-1/2}^n). \end{aligned} \quad (48)$$

Figures 5 and 6 show the staggered grid finite difference solutions with NPML. In all figures we show only the computational domain so reflected energy is easiest to see. We note that there is still substantial reflection back into the computational domain with the staggered grid scheme. These reflections are partly due to the same absorption coefficient ( $\eta = 250$ ) being used for this scheme as was used for the upscaling experiments even though it was only optimized for upscaling.

Next we discuss several experiments which show the result of using the upscaling algorithm with and without NPML. Pressure and acceleration are shown using the operator upscaling method for  $t \in [0, 1.026]$  s (up to 3000 time steps). As shown in Figure 7 (upsampling without NPML) the incident pressure wave reaches the edges of the computational domain at  $t = 0.342$  s

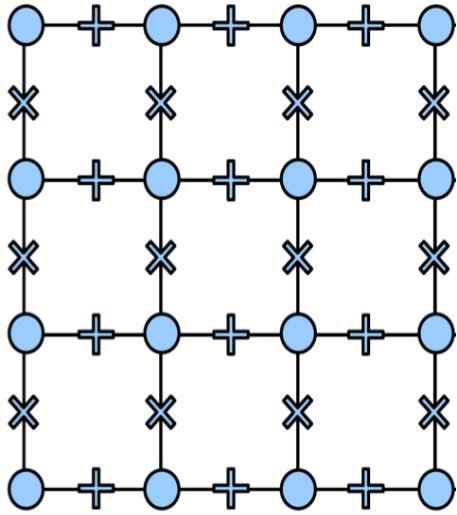


Fig. 4: Two-dimensional staggered-grid: Circles denotes pressure nodes, the ‘+’ denotes vertical acceleration nodes, and the ‘x’ denotes the horizontal acceleration nodes.

(1000th time step). Partial incident pressure wave energy begins to reflect back into the domain at subsequent time steps. The augmented or reconstructed acceleration solution from upscaling without NPML shown in Figure 8 is defined on the fine grid by

$$\mathbf{U} = \mathbf{U}^c + \delta\mathbf{U}. \quad (49)$$

In Figures 9 and 10 we show the effect of NPML on the upscaled solution (pressure and augmented acceleration respectively). The computational domain is defined to be the same size as in the previous example. However, in this experiment the total domain has been increased due to the addition of the NPML absorbing layer (150 fine grid points are added to each of the four boundaries of the computational domain). Thus the total domain has 2000 fine grid points in each direction (and 200 coarse grid points for upscaling). The maximum NPML decay factor,  $\eta$ , again has value 250. To examine the effectiveness of the NPML boundary conditions for Equations (1), we calculated the maximum relative reflected amplitude of the incident wave with respect to the Frobenius norm. We define the maximum relative reflected amplitude to be the ratio between the energy of the wave in the computational domain once the direct wave has completely exited the computational domain to the energy of the wave in the computational region at the time when the wave is first incident on the NPML boundary (1000th time step).

Maximum Relative Reflected Amplitude		
Time Step	Pressure	Acceleration
5000th (1.710 s)	0.03312	0.00097
6000th (2.052 s)	0.03297	0.00095

Table 1: Observed maximum relative reflected pressure and the  $x$ -component of acceleration from upscaling with NPML in a homogeneous medium at times  $t = 1.710$  s and 2.052 s.

In all the tables we used the  $x$  component of acceleration to calculate the reflected energy for acceleration. The maximum relative reflected pressure and acceleration amplitudes at time steps 5000 and 6000 are shown in Table 1. At the 5000th time step, the wave should ideally be completely contained in the NPML region. Clearly, both pressure and acceleration are absorbed in the NPML region. We note that pressure which is completely determined in the subgrid solve and to which we did explicitly apply NPML has a 3% reflection back into the computational domain. More significant is the fact that coarse acceleration which is not explicitly damped is very well absorbed. We see approximately 0.1% of the acceleration reflected back into the domain. At each time step the algorithm solves for subgrid unknowns using coarse acceleration and then updates coarse acceleration using the subgrid pressure and acceleration. This tight coupling between all three unknowns means the impact of NPML on reflected pressure and acceleration is complicated. Nonetheless, this implementation of NPML applied only to Step 1 of the two-step upscaling algorithm, does result in damping of the vast majority of the wave in the absorbing layer.

Next we examine the impact that the thickness of the NPML layer has on absorption. All parameters in this example are the same as in the previous example, except that the thickness of the absorbing layer varies from 50 to 250 fine grid points. As shown in Table 2, NPML regions larger than 150 grid points do not significantly reduce the relative reflected amplitude for pressure. However, NPML regions less than 150 fine grid points give greater reflection back into the computational domain. Finally in Table 3 we examine the impact changing the absorption coefficient has on the damping. For the homogeneous medium experiments we have chosen  $\eta = 250$  as this value of the absorption coefficient significantly reduces the relative reflection off the computational domain boundaries while not being so large as to potentially cause reflections off the interface between the computational region and the absorbing layer.

Maximum Relative Reflected Amplitude, t = 1.710 s		
NPML Size	Pressure	Acceleration
50	0.05864	0.00180
100	0.03488	0.00112
150	0.03312	0.00097
200	0.03276	0.00091
250	0.03244	0.00091
350	0.03192	0.00089

Table 2: Observed maximum relative reflected pressure and the  $x$ -component of acceleration from upscaling with NPML in a homogeneous medium at  $t = 1.710$  s for various NPML layer thicknesses.

Maximum Relative Reflected Amplitude, t = 1.710 s	
Absorption Coefficient	Pressure
50	0.12398
250	0.03312
$10^3$	0.03356
$10^5$	0.03329
$10^7$	0.03482
$10^9$	0.81230

Table 3: Observed maximum relative reflected pressure amplitudes from upscaling with NPML in a homogeneous medium at  $t = 1.710$  s for various values of the absorption coefficient.

## 4.2 Heterogeneous Medium Experiments

In this section, we describe two heterogeneous medium experiments to test the effectiveness of the NPML implementation on the upscaling algorithm. For these two experiments, the computational domain and spatial grid spacing are the same as for the homogeneous medium experiments. The time step is chosen to satisfy the CFL condition. In order to reduce reflections while minimizing the size of the absorbing layer, the NPML region is again chosen to be 150 fine grid points on each of the four edges of the computational domain. Thus the total domain (computational plus absorbing layer) is 2 km x 2 km (2000 x 2000 fine grid points, 200 x 200 coarse grid points). The time step is  $\Delta t = 8.839 \times 10^{-5}$  s. The maximum NPML decay factor,  $\eta$ , was increased to 1000. In the first experiment, thin strips of varying velocity values are overlain on a homogeneous background velocity of 2500 m/s. The thin velocity strips increase from the top of the domain to the bottom with values ranging from 2750 m/s to 7500 m/s. Each thin strip is 3 m (3 fine grid blocks) wide which is considerably below the size of a single coarse block (10 m in each direction). This experiment is similar to Experiment 3 in Vdovina et al. [33]. The input velocity field for this first heterogeneous medium experiment is shown in Figure 11. We note that our objective here is not to test whether the upscaling method works well, but rather to show that our NPML implementation with operator upscaling effectively damps reflected energy off the computational

domain boundaries. Earlier papers (see [33, 32]) demonstrate that the operator upscaling method captures sub-wavelength heterogeneities in the solution. The incident pressure wave first hits the NPML interface at  $t = 0.354$  s (time step 4000). We note that unlike in the homogeneous case, energy can reflect off of internal layers and so the energy does not completely leave the domain until much later than in the homogeneous experiment. In fact it can be difficult to determine the right time to estimate the reflected energy in order to avoid including a portion of the wave which has not yet left the computational region in the estimate of the reflected energy. Consequently, we ran the first heterogeneous medium experiment for 15,000 time steps total. The relative reflected energy is computed as a ratio of the energy at the 15,000th time step to the energy when the wave first impinges on the computational domain boundary. The maximum reflected energy for pressure is 0.057 and for acceleration is 0.0077 (see Table 4). In Figures 12, 13, and 14, we show the effect of NPML on the upscaled solution in the first heterogeneous medium experiment. Since the velocity field is homogeneous in the x-direction, the horizontal acceleration does not see the thin layer interfaces in sound velocity (see Figure 13). However, the impact of this thin layering is clearly seen in the vertical acceleration shown in Figure 14. The upscaling captures fine-scale fluctuations in sound velocity, and the NPML absorbs the vast majority of potential artificial reflections from the edges of the computational domain.

In the second experiment, the velocity field consists of two pieces: a layered background with varying layer thickness and superimposed on that layered background is a velocity perturbation generated from the Karhunen-Loéve Expansion (KLE) (see [21, 30]). The stochastic velocity perturbation results from a 100-term KLE expansion with 100 m correlation length and a 1500 m/s standard deviation. The velocity field for heterogeneous experiment 2 is shown in Figure 15. The time step is taken to be  $\Delta t = 6.529 \times 10^{-5}$  s. For this experiment we show only the pressure in Figure 16. The incident wave takes much longer to reach the NPML region due to the highly heterogeneous medium. Thus the reflected energy is defined to be the ratio of energy in the computational domain at time step 20,000 to the energy in the computational region when the wave impinges on the computational domain boundary. The maximum relative reflected pressure and acceleration amplitudes for these experiments are shown in Table 4. For pressure the relative reflected energy is 0.082 and for acceleration it is 0.009.

Maximum Relative Reflected Amplitude		
Experiment	Pressure	Acceleration
Thin Layered	0.05739	0.00766
Stochastic Perturbation	0.08156	0.00919

Table 4: Observed maximum relative reflected pressure and the  $x$ -component of acceleration for the heterogeneous medium experiments.

## 5 Conclusion

For upscaling schemes to be useful as forward simulators for inversion, it is imperative that artificial reflections off computational domain boundaries are minimized. In this paper we have adapted NPML for use with one particular upscaling method (operator upscaling for the acoustic wave equation). The upscaling method has two steps (a subgrid solve and a coarse solve) which are tightly coupled at each time step. We found that applying NPML to the first stage of the two stage algorithm was sufficient to damp both pressure and acceleration even in the second step of the algorithm (coarse acceleration). Due to the property that within the computational domain the NPML equations are the same as the original governing equations, parallelization of the subgrid stage of the operator upscaling method is unaffected. An optimal thickness of the absorbing layer and the absorption coefficient for these experiments is found through computational experiments. Pressure showed the most reflection back into the computational domain (3–8%). Even without explicit damping of coarse acceleration in our two step algorithm with NPML, only 0.1–1% of acceleration is reflected. These experiments indicate the effectiveness of implementing NPML on the fine grid only for upscaling. Different upscaling methods would likely require different approaches, but this study provides at least some insight into how to approach reduction of artificial reflections when using upscaling for the wave equation.

## 6 Acknowledgments

We thank two anonymous reviewers for helpful comments that improved the manuscript.

## References

1. Arbogast, T.: Analysis of a two-scale, locally conservative subgrid upscaling for elliptic problems. *SIAM J. Numer. Anal.* **42**, 576–598 (2004)
2. Arbogast, T., Minkoff, S., Keenan, P.: An operator-based approach to upscaling the pressure equation. *Computational Methods in Water Resources XII: Computational Mechanics Publications* **V. Burganos, G. Karatzas, A. Payatakes, C. Brebbia, W. Gray, and G. Pinder, Eds.**, 405–412 (1998)
3. Berenger, J.P.: A perfectly matched layer for the absorption of electro-magnetic waves. *Journal of Computational Physics* **114**, 185–200 (1994)
4. Bermdez, A., Hervella-Nieto, L., Prieto, A., Rodriguez, R.: An optimal finite-element/PML method for the simulation of acoustic wave propagation phenomena. *Variational Formulation in Mechanics: Theory and Applications* **E. Taroco et al. eds**, 43–54 (2007)
5. Christie, M.: Upscaling for reservoir simulation. *J. Pet. Tech.* **48**, 1004–1010 (1996)
6. Chung, E., Efendiev, Y., Gibson, R.: Multiscale finite element modeling of acoustic wave propagation. In: *SEG Technical Program Expanded Abstracts*, pp. 2898–2903. Society of Exploration Geophysicists (2011)
7. Clayton, R., Engquist, B.: Absorbing boundary conditions for acoustic and elastic wave equations. *Bulletin of the Seismological Society of America* **67**, 1529–1540 (1977)
8. Cohen, G.: Higher order numerical methods for transient wave equations. Springer-Verlag, New York (2002)
9. Cummer, S.: A simple, nearly perfectly matched layer for general electromagnetic media. *IEEE Microwave and Wireless Components Lett.* **13**, 137–140 (2003)
10. Durlofsky, L.: Numerical calculation of equivalent grid block permeability tensors for heterogeneous porous media. *Water Resour. Res.* **27**, 699–708 (1991)
11. E, W., Engquist, B.: Multiscale modeling and computation. *Notices of the American Math Society* **50**, 1062–1070 (2003)
12. E, W., Engquist, B., Huang, Z.: Heterogeneous multiscale method: A general methodology for multiscale modeling. *Physical Review* **67**, 092,101–1–092,101–4 (2003)
13. Fokkema, J.T., Van den Berg, P.M.: *Seismic Applications of Acoustic Reciprocity*. Elsevier, Amsterdam (1993)
14. Gibson, R., Gao, K., Chung, E., Efendiev, Y.: Multiscale modeling of acoustic wave propagation in 2d media. *Geophysics* **79**(2), T61–T75 (2014)

15. Givoli, D., Keller, J.B.: Non-reflecting boundary conditions for elastic waves. *Wave Motion* **12**, 261–279 (1990)
16. Givoli, D., Vigdergauz, S.: Artificial boundary conditions for 2D problems in geophysics. *Computer Methods in Applied Mechanics and Engineering* **110**, 87–101 (1993)
17. Grote, M., Keller, J.B.: Exact nonreflecting boundary condition for elastic waves. *SIAM Journal on Applied Mathematics* **60**, 803–819 (2000)
18. He, F., Ruiz, C., Becker, A.: Absorbing boundaries in numerical solutions of the time-dependent Schrodinger equation on a grid using exterior complex scaling. *J. Phys. Rev. A.* **75**, 353–407 (2007)
19. Hu, H., Cummer, S.A.: The nearly perfectly matched layer is a perfectly matched layer. *IEEE Antennas and Wireless Propagation Lett.* **3**, 137–140 (2004)
20. Hu, W., Abubakar, A., Habashy, T.: Application of the nearly perfectly matched layer in acoustic wave modeling. *Geophysics* **72**, 169–175 (2007)
21. Huang, S.P., Quek, S.T., Phoon, K.K.: Convergence study of the truncated Karhunen-Loéve expansion for simulation of stochastic processes. *International Journal for Numerical Methods in Engineering* **52**(9), 1029–1043 (2001)
22. Johnson, S.: Notes on Perfectly Matched Layers (PMLs) (2010). <http://math.mit.edu/~stevenj/18.369/pml.pdf>
23. Jones, F.: Lebesgue Integration On Euclidean Space. Jones & Bartlett Learning, Boston (2000)
24. Katz, D.C., Thiele, E.T., Taflove, A.: Validation and extension to three dimensions of the Berenger absorbing boundary condition for fdtd meshes. *IEEE Microwave Guided Wave Lett.* **4**, 268–270 (1994)
25. King, P., Williams, J.: Upscaling permeability: Mathematics of renormalization. *Transp. Porous Media* **23**, 337–354 (1996)
26. Korostyshevskaya, O., Minkoff, S.: A matrix analysis of operator-based upscaling for the wave equation. *SIAM J. Numer. Anal.* **44**(2), 586–612 (2006)
27. Kosloff, R.: Absorbing boundaries for wave propagation problems. *J. Comput. Phys.* **63**, 363–376 (1986)
28. Nunes, V., Minkoff, S.E.: Imaging via subgrid upscaling and reverse time migration. In: SEG Technical Program Expanded Abstracts, pp. 4008–4013. Society of Exploration Geophysicists (2014)
29. Russell, T., Wheeler, M.: The mathematics of reservoir simulation. SIAM (1983)
30. Stuart, G., Yang, W., Minkoff, S., Pereira, F.: A two-stage Markov chain Monte Carlo method for velocity estimation and uncertainty quantification. *Proceedings of the 86th Annual International Meeting of the Society of Exploration Geophysicists* pp. 3682–3687 (2016)
31. Vdovina, T., Minkoff, S.: An a priori error analysis of operator upscaling for the acoustic wave equation. *International Journal of Numerical Analysis and Modeling* **5**, 543–569 (2008)
32. Vdovina, T., Minkoff, S., Griffith, S.: A twoscale solution algorithm for the elastic wave equation. *SIAM Journal on Scientific Computing* **31**, 3356–3386 (2009)
33. Vdovina, T., Minkoff, S., Korostyshevskaya, O.: Operator upscaling for the acoustic wave equation. *SIAM J. Multiscale Model. Simul.* **4**, 1305–1338 (2005)
34. Zhou, W., Brossier, R., Operto, S., Virieux, J.: Acoustic multiparameter full-waveform inversion through a hierarchical scheme. In: SEG Technical Program Expanded Abstracts, pp. 1249–1253. Society of Exploration Geophysicists (2014)

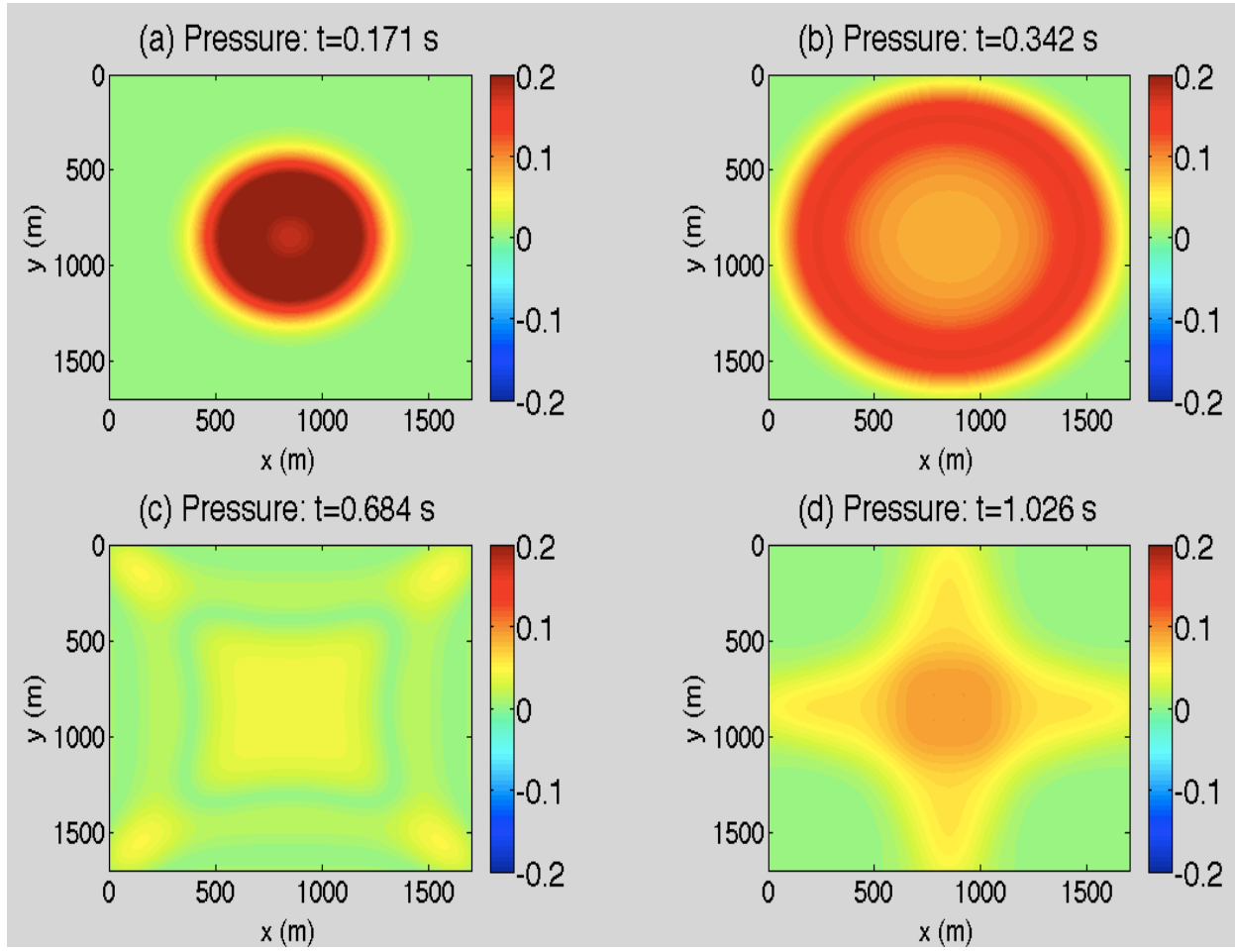


Fig. 5: Pressure solution from the staggered grid finite difference scheme with NPML but without upscaling. The medium is homogeneous, and the solution is shown at times  $t =$  (a) 0.171 s, (b) 0.342 s, (c) 0.684 s, and (d) 1.026 s.

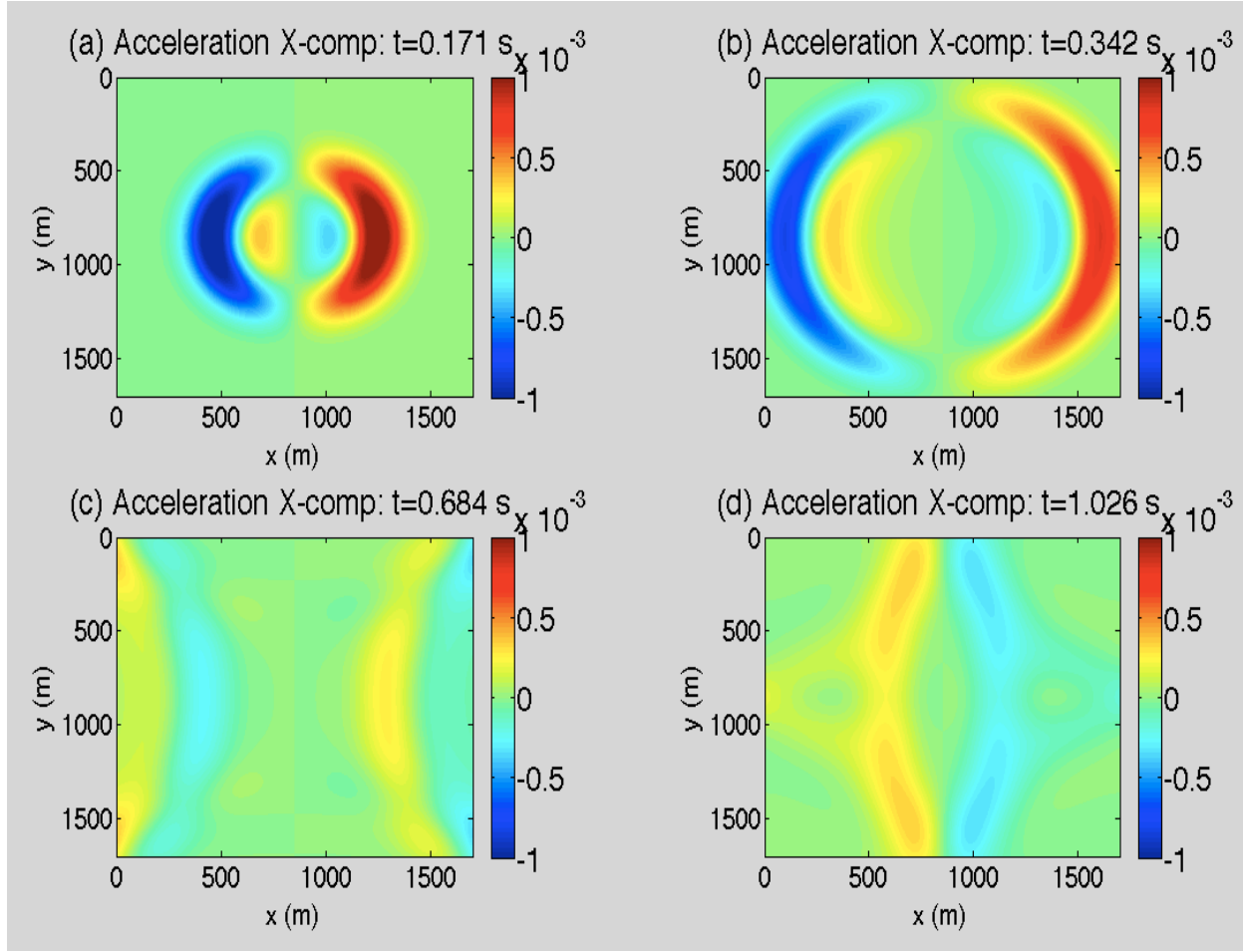


Fig. 6: Acceleration on the fine grid using a staggered grid finite difference scheme with NPML but without upscaling. The medium is homogeneous, and the solution is shown at times  $t =$  (a)  $0.171 \text{ s}$ , (b)  $0.342 \text{ s}$ , (c)  $0.684 \text{ s}$ , and (d)  $1.026 \text{ s}$ .

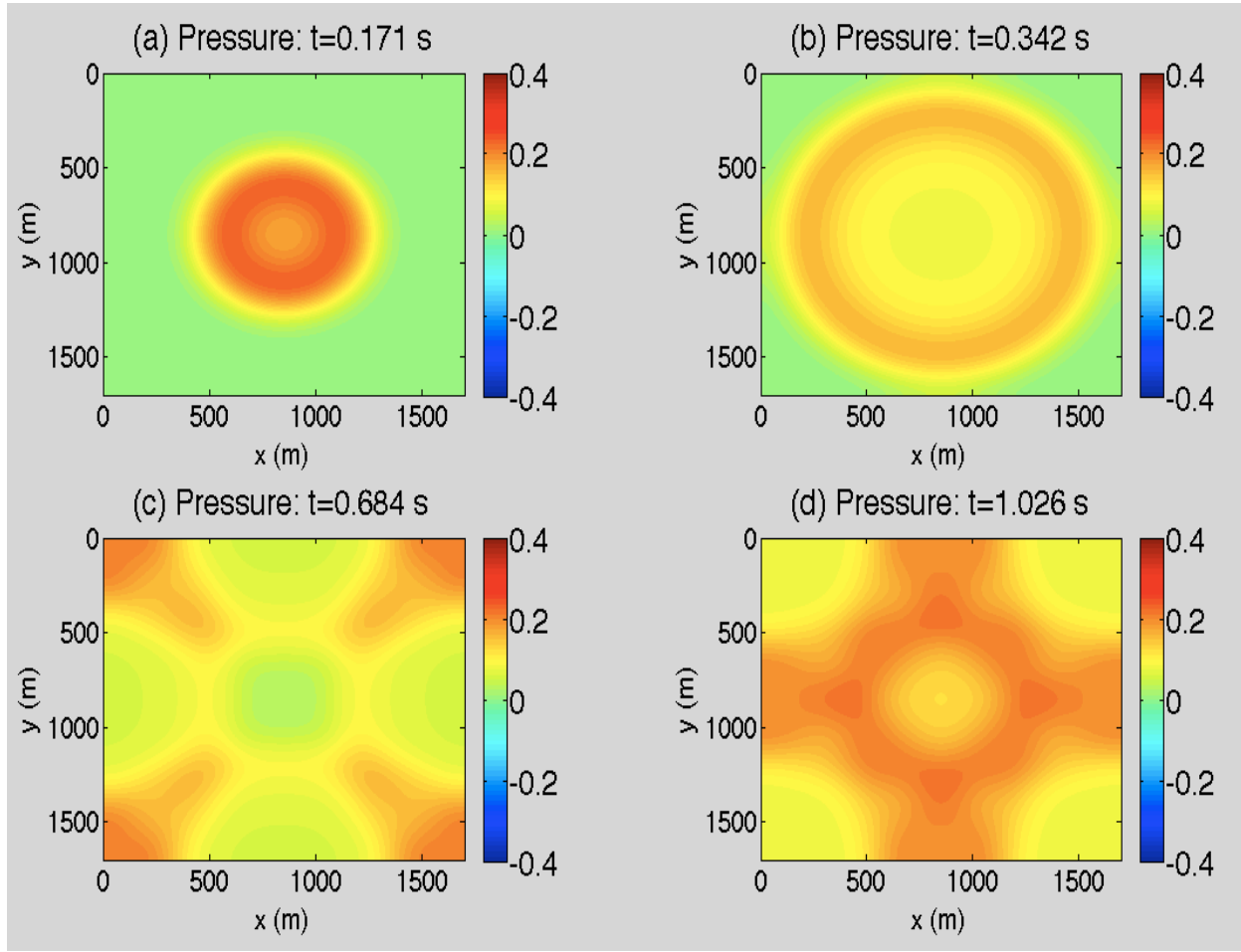


Fig. 7: Pressure solution from upscaling without NPML in a homogeneous medium at four distinct times: (a)  $t = 0.171$  s (500th time step), (b)  $t = 0.342$  s (1000th time step), (c)  $t = 0.684$  s (2000th time step), and (d)  $t = 1.026$  s (3000th time step). The incident pressure wave reaches the edge of the computational domain at  $t = 0.342$  s and reflects back into the domain.

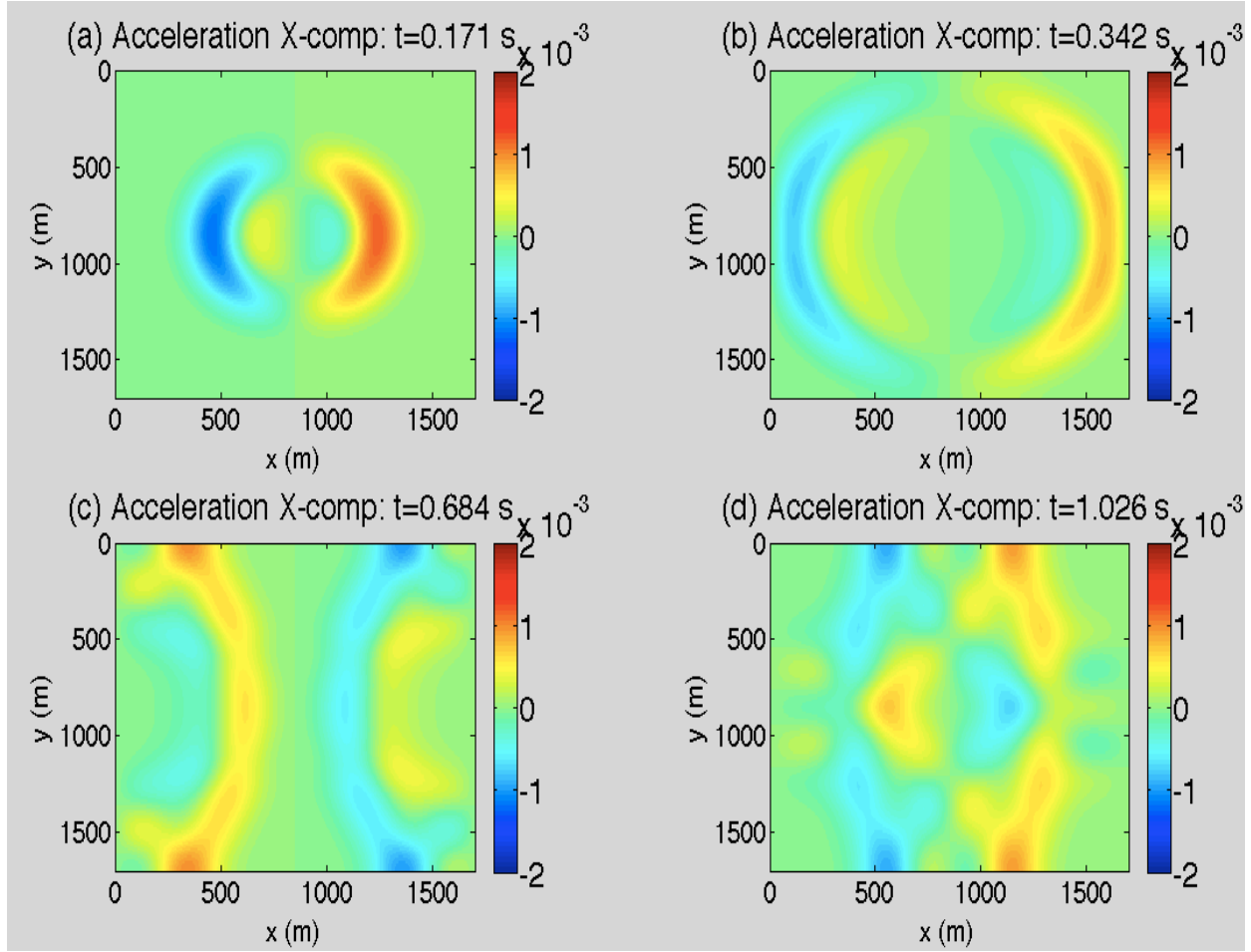


Fig. 8: The  $x$ -component of the augmented acceleration solution from upscaling without NPML in a homogeneous medium is shown at times (a)  $t = 0.171 \text{ s}$ , (b)  $t = 0.342 \text{ s}$ , (c)  $t = 0.684 \text{ s}$ , and (d)  $t = 1.026 \text{ s}$ . The wave reaches the edge of the computational domain at  $t = 0.342\text{s}$ .

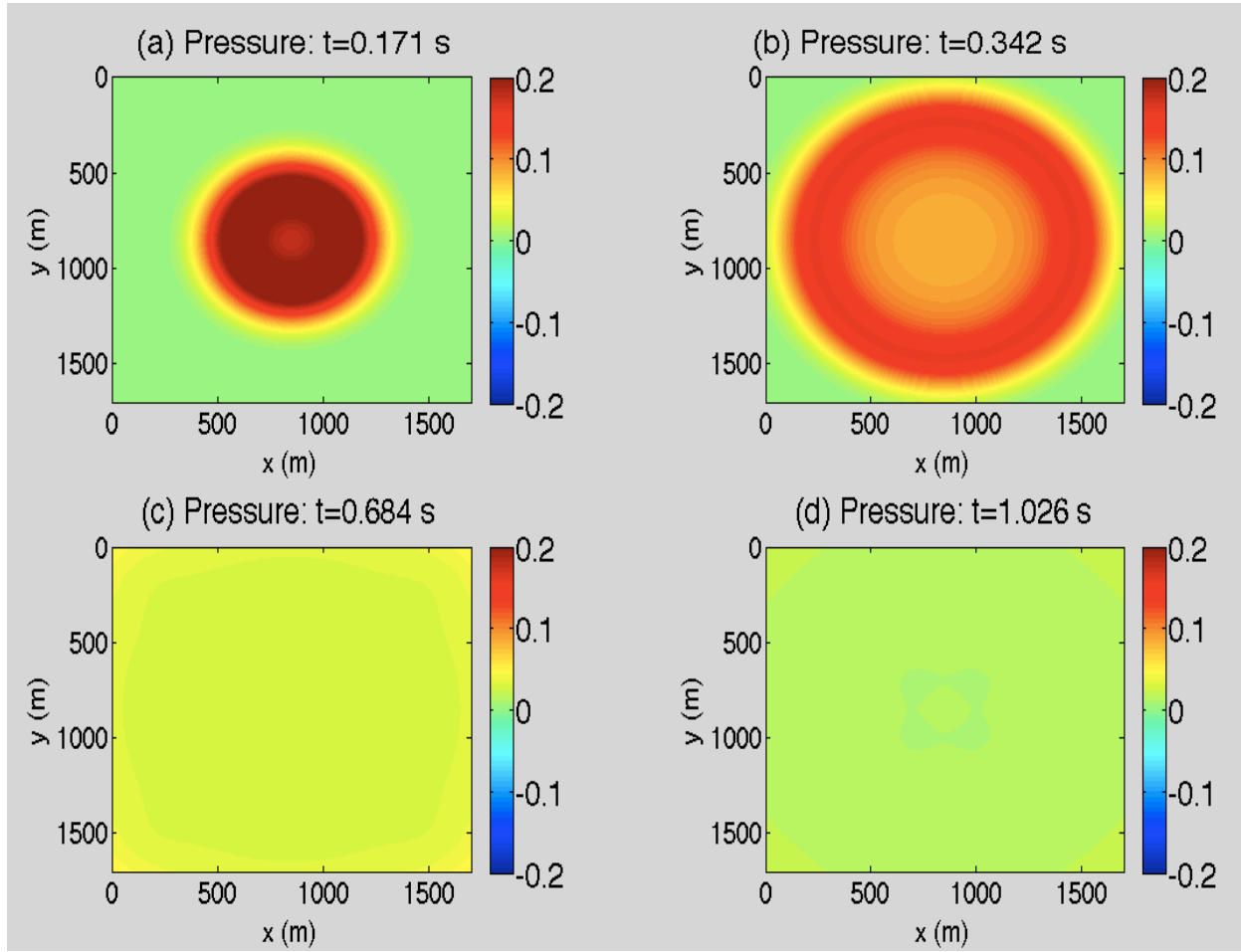


Fig. 9: Pressure solution from upscaling with NPML in a homogeneous medium at times  $t =$  (a) 0.171 s, (b) 0.342 s, (c) 0.684 s, and (d) 1.026 s. The computational domain is defined to be 1.7 km  $\times$  1.7 km with an absorbing layer of 150 m on each edge of the 2D domain. Overall, pressure is absorbed in the NPML region. Only the computational region is shown in the figure.

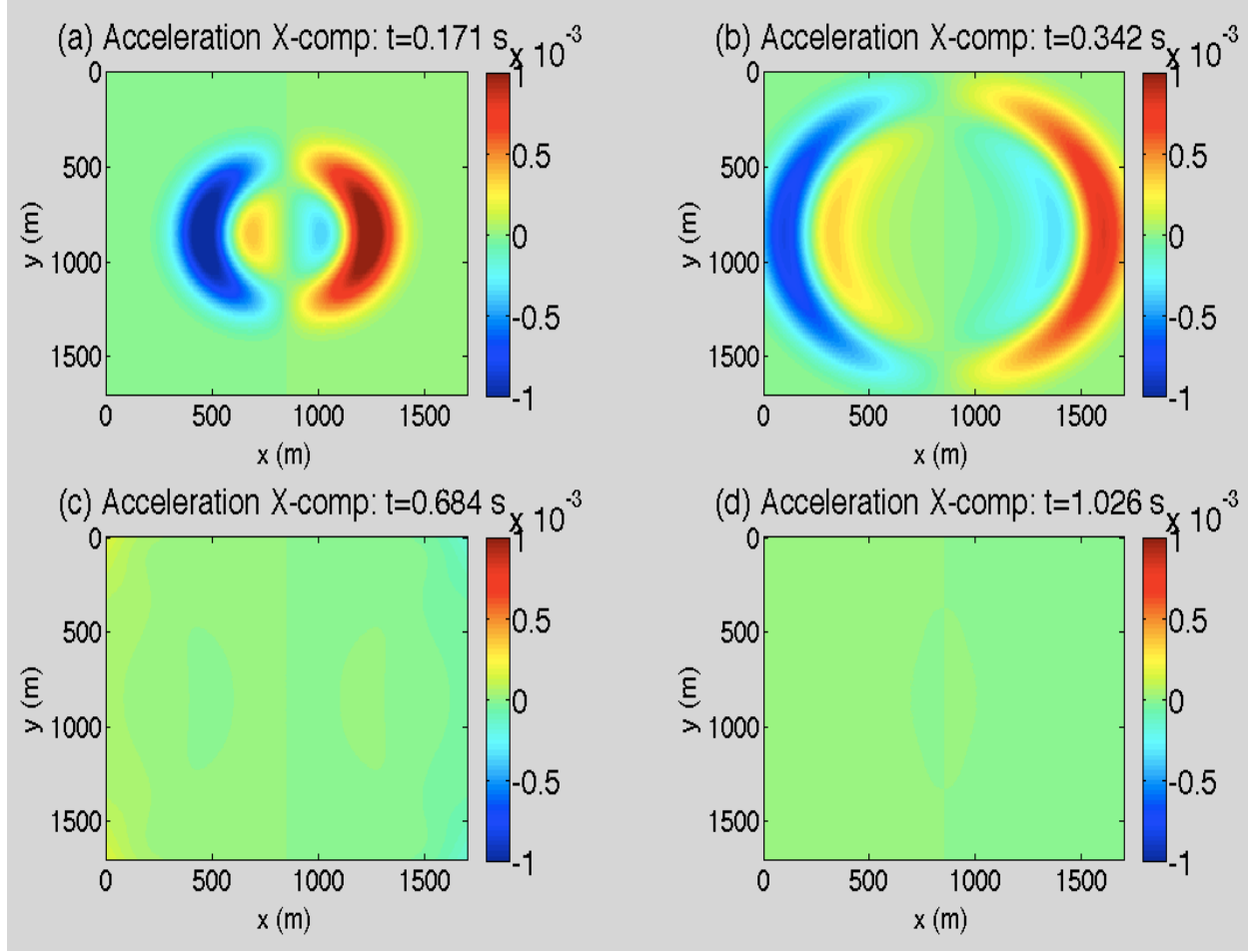


Fig. 10: The  $x$ -component of the augmented acceleration from upscaling with NPML in a homogeneous medium for times  $t =$  (a)  $0.171 \text{ s}$ , (b)  $0.342 \text{ s}$ , (c)  $0.684 \text{ s}$ , and (d)  $1.026 \text{ s}$ . Overall, the acceleration (both coarse and fine) are absorbed in the NPML region. Only the computational region is shown in the figure.

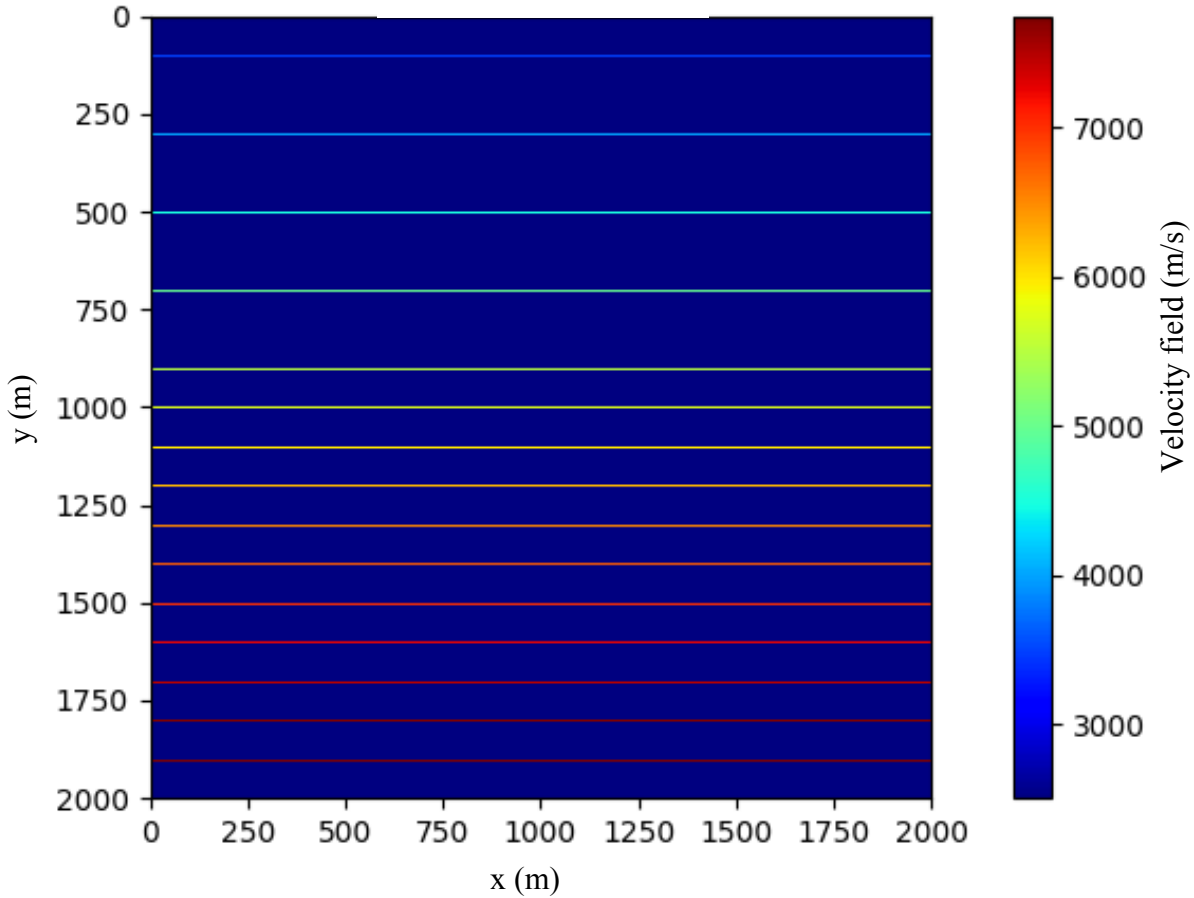


Fig. 11: The input velocity field for the first heterogeneous medium experiment in which thin velocity strips 3 fine grid blocks wide are embedded in a homogeneous background medium. The coarse grid blocks contain 10 fine grid blocks in each direction.

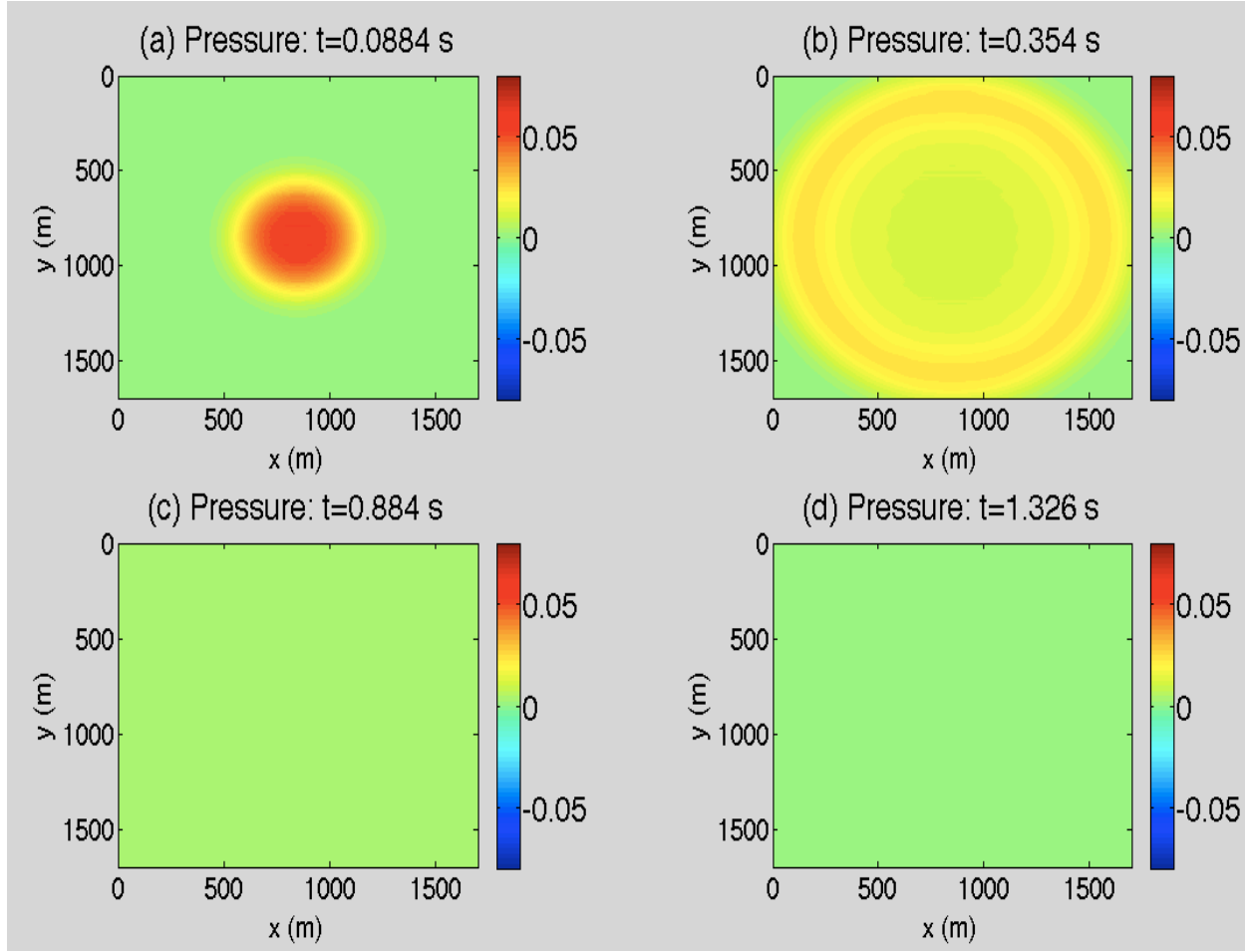


Fig. 12: Pressure solution from upscaling with NPML for the first heterogeneous medium experiment corresponding to the velocity field shown in Figure 11 at times  $t =$  (a) 0.0884 s, (b) 0.354 s, (c) 0.884 s, and (d) 1.326 s. The computational domain is defined to be 1.7 km x 1.7 km with an absorbing layer of 150 m on each edge of the 2D domain. Only the computational region is shown in the figure.

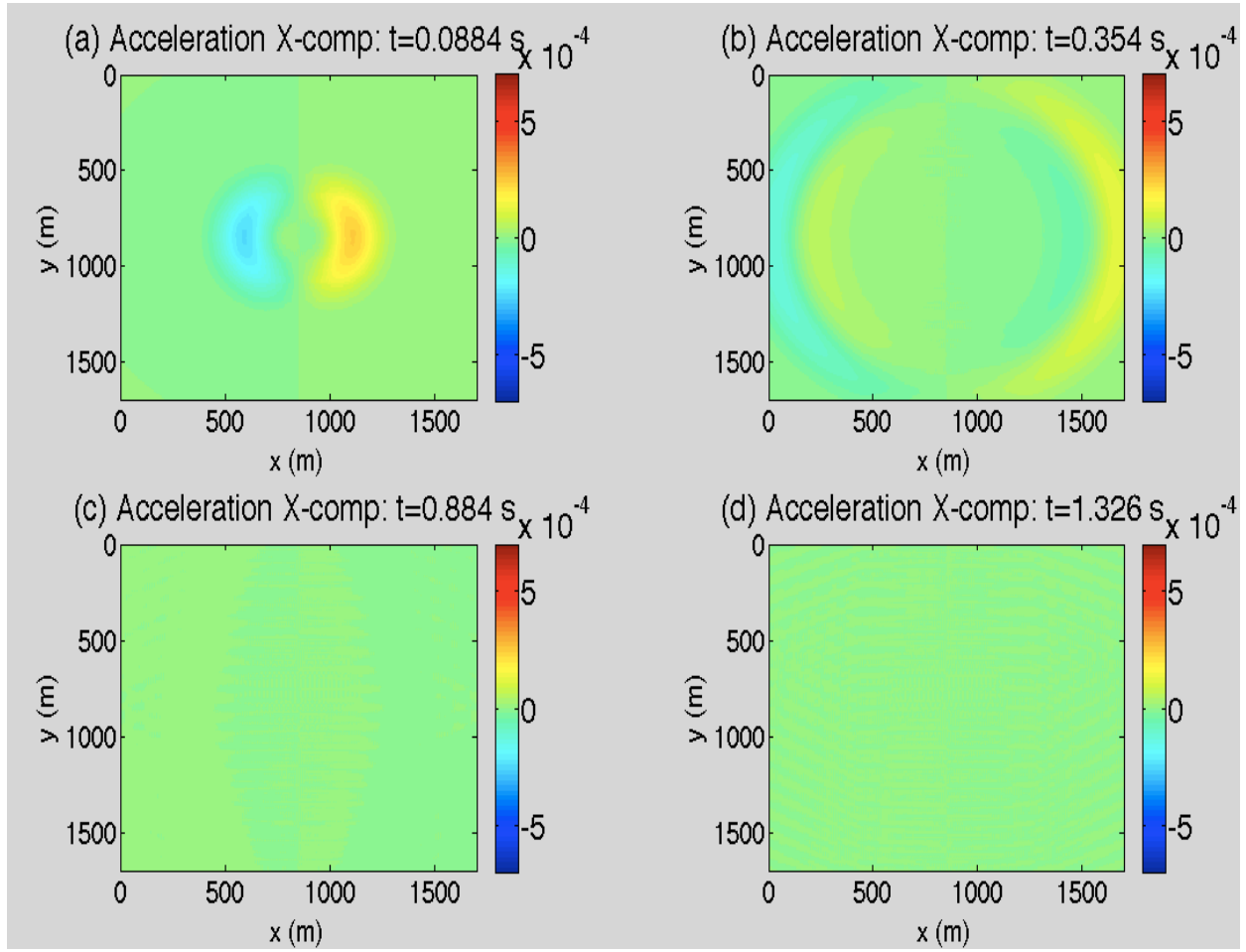


Fig. 13: The  $x$ -component of the augmented acceleration from upscaling with NPML for the heterogeneous experiment corresponding to the velocity field shown in Figure 11 for times  $t =$  (a) 0.0884 s, (b) 0.354 s, (c) 0.884 s, and (d) 1.326 s. Overall, the acceleration (both coarse and fine) are absorbed in the NPML region. Only the computational region is shown in the figure.

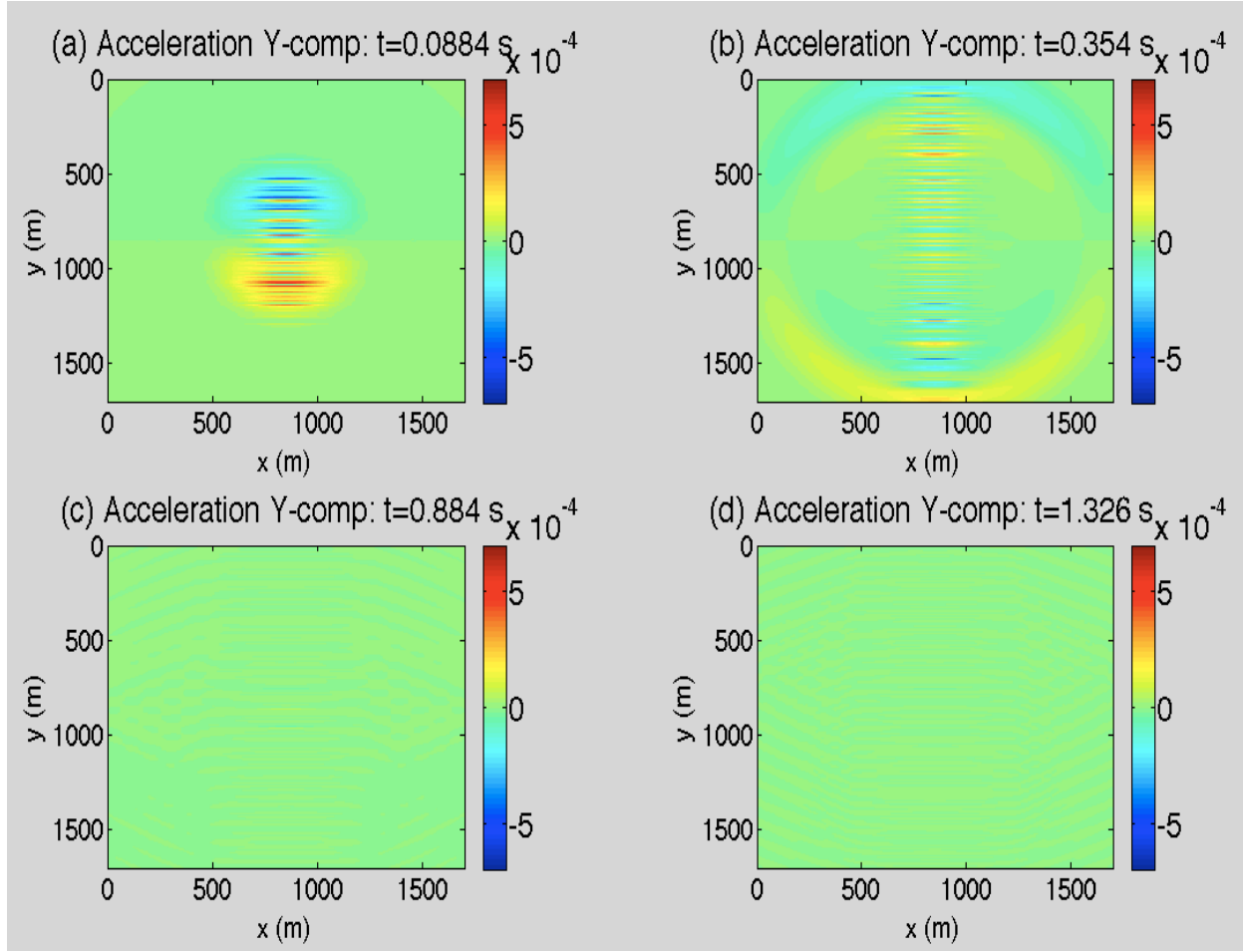


Fig. 14: The  $y$ -component of the augmented acceleration from upscaling with NPML for the heterogeneous experiment corresponding to the velocity field shown in Figure 11 at times  $t =$  (a) 0.0884 s, (b) 0.354 s, (c) 0.884 s, and (d) 1.326 s. The vertical acceleration captures the fine-scale fluctuations in sound velocity. Only the computational region is shown in the figure.

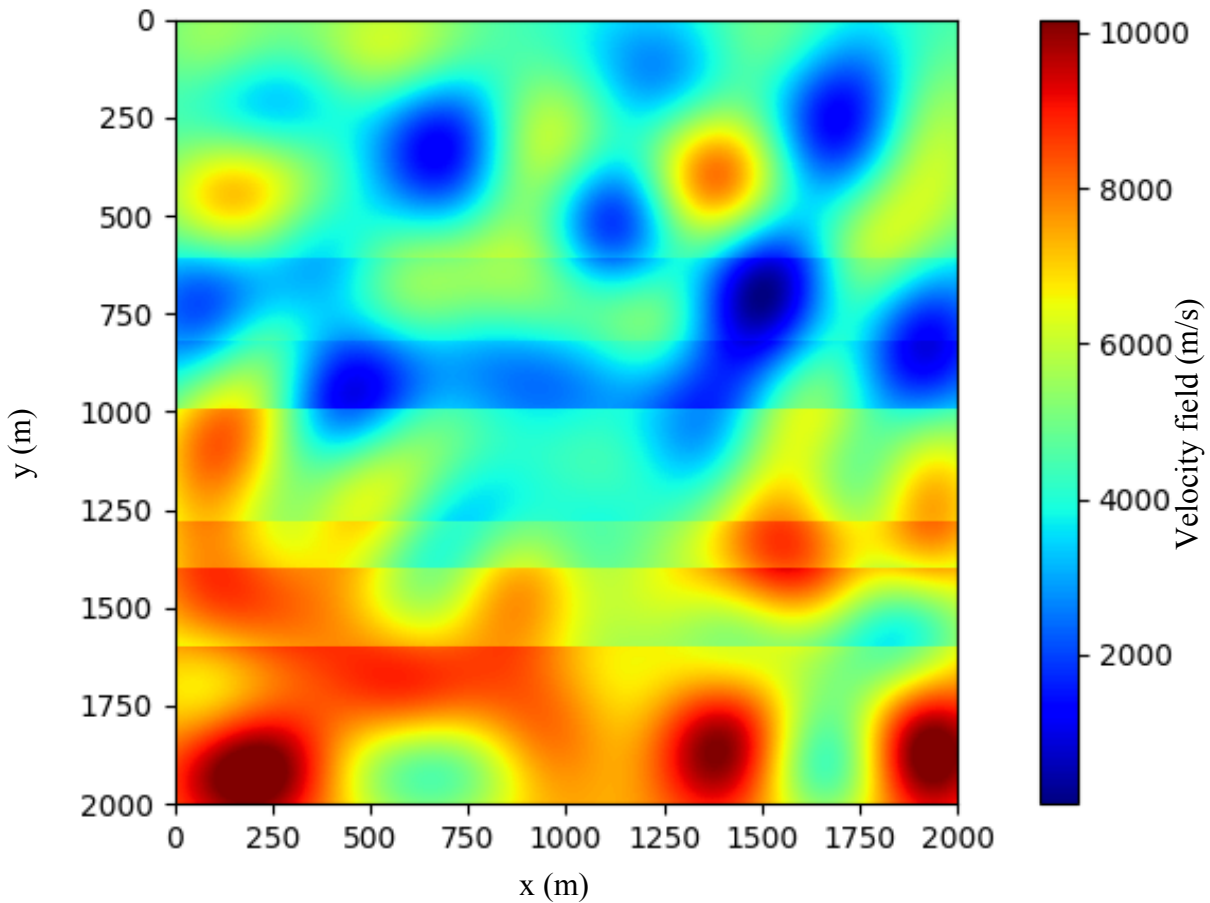


Fig. 15: The input velocity field for the second heterogeneous medium experiment in which a stochastic perturbation to velocity is overlaid on a layered background.

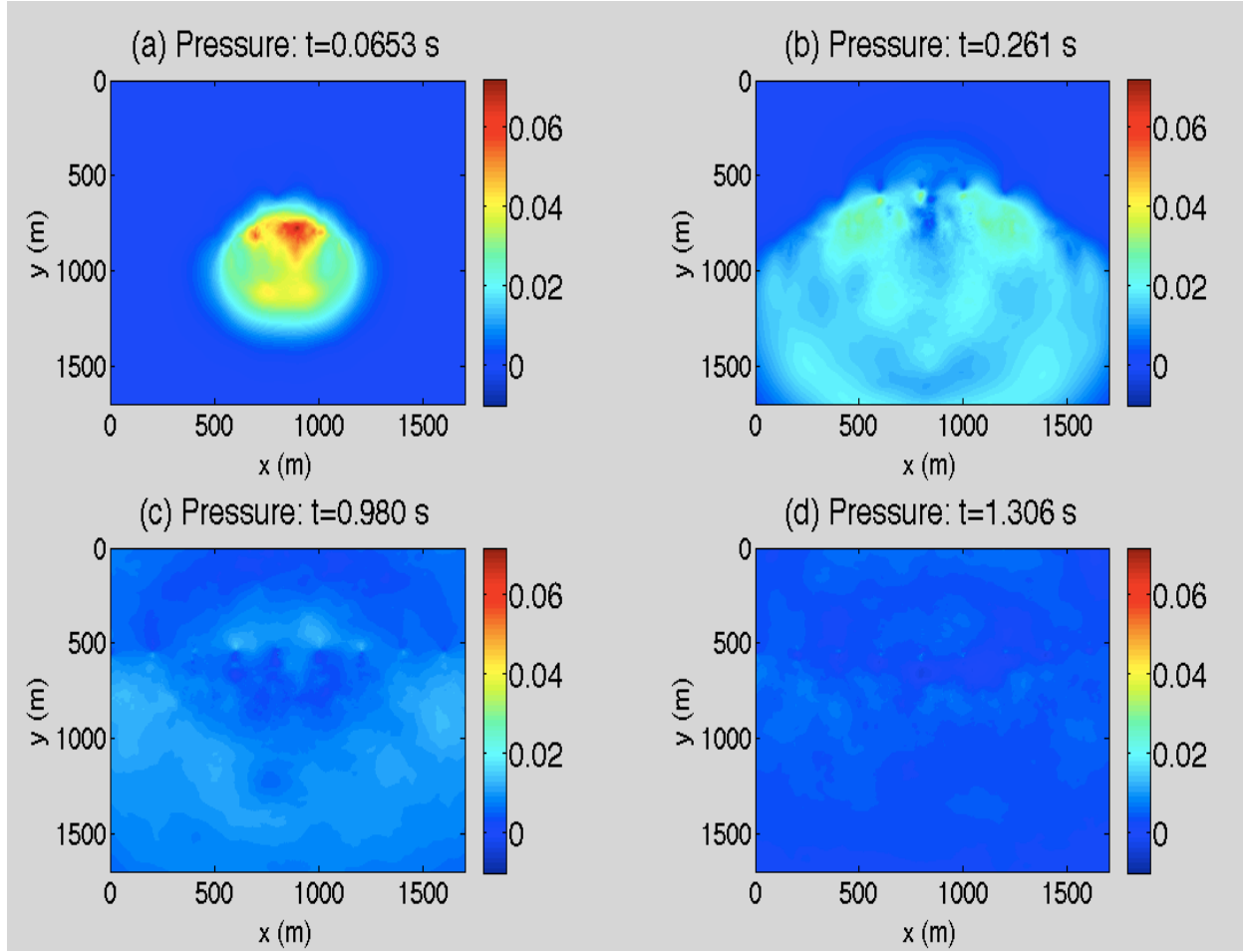


Fig. 16: Pressure solution from upscaling with NPML for the second heterogeneous medium experiment. The velocity field for this experiment is shown in Figure 15. Pressure is shown at times  $t =$  (a) 0.0653 s, (b) 0.261 s, (c) 0.980 s, and (d) 1.306 s. The computational domain is defined to be 1.7 km x 1.7 km with an absorbing layer of 150 m on each edge of the 2D domain. Only the computational region is shown.